Solids back-mixing in the transport zone of circulating fluidized bed boilers

Chemical Engineering Journal 428 (2022) 130976

Contents lists available at ScienceDirect

Chemical Engineering Journal

journal homepage: www.elsevier.com/locate/cej

Solids back-mixing in the transport zone of circulating fluidized bed boilers

Tove Djerf [a], David Pallarès [a,*], Filip Johnsson [a], Gaetano Sardina [b], Henrik Ström [b]

[a] Department of Space, Earth and Environment, Chalmers University of Technology, 412 96 Göteborg, Sweden
[b] Department of Mechanics and Maritime Sciences, Chalmers University of Technology, 412 96 Göteborg, Sweden

ARTICLE INFO

Keywords:
Circulating fluidized bed
Lateral dispersion
Solids back-mixing
Deposition velocity

ABSTRACT

This work investigates the back-mixing of solids in the transport zone of large-scale circulating fluidized bed (CFB) boilers, with the aims of identifying and evaluating the governing mechanisms and providing a mathematical description based on a solid theoretical background rather than on purely empirical correlations. In addition, transient Direct Numerical Simulation (DNS) modeling is used to identify the mechanism that drives migration of the solids from the dilute up-flow in the core region to the down-flow at the furnace walls. Previously published concentration and pressure profiles are collated and analyzed through modeling of the steady-state mass balance of the dispersed solids in the transport zone. The study shows that solids back-mixing at the furnace wall layers is limited (hence governed) by the core-to-wall layer mass transfer transport mechanism rather than by the lateral movement of solids within the core region. The latter is shown by the 3-dimensional (3D) mass balance model, and the transient DNS modeling indicates that this is due to a turbophoresis mechanism. We also show that the use of *Pe*-numbers to describe the lateral solids dispersion is not straightforward but rather depends on the unit scale, and that *Pe-numbers* < 26 are needed to yield the solids back-mixing rates measured in large-scale CFB boilers. Finally, we propose a mathematical expression for the core-to-wall layer mass transfer coefficient derived from a Sherwood number (*Sh*)-correlation fitted to measured values of the characteristic decay constant that result from the solids back-mixing. This expression shows better agreement with the large-scale measurements than do the expressions given in the literature.

1. Introduction

The mitigation of anthropogenic global warming and the need for a reliable energy supply are key drivers of technical developments in the heat and power sectors. In addition, higher levels of efficiency, larger shares of renewables, and the implementation of carbon capture and storage processes are among the necessary measures for meeting the goals set in the Paris Agreement [1]. In this context, fluidized bed combustion is a widely used technology with strong fuel flexibility [2,3]. It has been shown to convert efficiently renewable fuels, such as biomass and selected waste fractions, and low-rank fuels with low calorific values (often coupled to having high levels of moisture and/or ash contents) [4]. Furthermore, several carbon capture technologies are strongly linked to fluidized bed units [5], either as the technologic basis (chemical looping, calcium looping) or as an option for compact furnace designs (oxyfuel) [6].

Circulating fluidized bed (CFB) combustion is carried out at higher gas velocities than are used in the traditional bubbling fluidized bed combustors. Thus, CFB combustors offer higher specific thermal power while entailing significant solids flows throughout the furnace. The further development of the CFB combustion technology requires increased knowledge of the solids mixing patterns, as these govern the heat transfer and, thereby, the closure of the heat balance. Unfortunately, the relatively large volumes of experimental data available from laboratory-scale units cannot be used directly for the study of large-scale boilers because the solids flow patterns differ significantly between these two unit scales [7,8], preventing direct scale-up [9,10]. While considerable efforts have been made to develop models from first principles, CFD modeling is still not an efficient tool for describing large-scale CFB combustion. This is a consequence of either highly uncertain formulations of some terms in the momentum equation (for the Eulerian description of the particulate phase) or limitations linked to computing capacity (for the Lagrangian approach) [11]. Thus, the development of CFB combustion relies heavily on semi-empirical models that ensure closure of the mass and heat balances at the macroscopic scale with the support of observations derived from large-scale measurements.

Based on measurements performed in a 12-MW^{th} CFB boiler, Johnsson and Leckner [12] divided the solids flow in large-scale CFB furnaces into three fluid-dynamical regions: (i) the dense bottom bed

* Corresponding author.
E-mail addresses: atovek@chalmers.se (T. Djerf), david.pallares@chalmers.se (D. Pallarès).

https://doi.org/10.1016/j.cej.2021.130976
Received 8 April 2021; Received in revised form 18 June 2021; Accepted 19 June 2021
Available online 3 July 2021

Notation

A	Cross-sectional area [m^2]
C_1	Constant [-]
C_s	Concentration of particles [kg/m^3]
$C_{s,max}$	Maximum concentration of solids in the transport zone [kg/m^3]
$C_{s,min}$	Minimum concentration of solids in the transport zone [kg/m^3]
d_p	Particle diameter [mm]
D_g	Gas dispersion [m^2/s]
$D_{s,lat}$	Solids macroscopic dispersion in the lateral direction [m^2/s]
F	Flux of particles [kg/s]
g	Gravity constant, 9.81 [m/s^2]
G_s	External circulation of solids [kg/m^2s]
h	Height over distributor plate [m]
H_t	Height of boiler [m]
k	Mass transfer coefficient [m/s]
K	Decay coefficient in the transport zone [m^{-1}]
K_{max}	Maximum decay coefficient of the transport zone [m^{-1}]
K_{min}	Minimum decay coefficient of the transport zone [m^{-1}]
L_x or L_y	Dimensions of units [m]
l_e	Size of turbulent eddies [m]
ΔP	Differential pressure [kPa]
r	Clustering at a net volumetric rate [1/s]
t	Time [s]
u' or v'_y	Amplitude of the velocity fluctuations [m/s]
u^*	Shear velocity [m/s]
u_g	Fluidization velocity [m/s]
$u_{s,Dlat}$	Characteristic velocity for the lateral dispersion of solids [m/s]
u_t	Terminal velocity of particles [m/s]
U	Velocity [m/s]

Greek letters:

$\varnothing_h$	*H*ydraulic diameter, $4L_xL_y/(2L_x + 2L_y)$ [m]
δ_{wall}	Wall layer thickness [mm]
ε_g	Gas fraction [-]
ε_s	Particle fraction [-]
μ_g	Gas viscosity [Pas]
ν_g	Kinematic viscosity of gas [m^2/s]
ρ_g	Density of gas [kg/m^3]
ρ_s	Density of solid particles [kg/m^3]
τ_V^*	Dimensionless relaxation time [-]
τ	Relaxation time [s]

Dimensionless number

Re	Reynolds particle number, $\frac{\varnothing_h(u_g-u_t)\rho_g}{\mu_g}$
Sc	Schmitt number, $\frac{\mu_g}{\rho_g D_{s,lat}}$
St	Stokes number
Pe	Peclet number, $\frac{u_g \varnothing_h}{D_{s,lat}}$
Sh	Sherwood number, $\frac{k\varnothing_h}{D_{s,lat}}$

(with a typical bed height of only a few decimeters, although it can be depleted at sufficiently low riser pressure drops [13]); (ii) the splash zone (located immediately above the dense bed and populated mostly by clustered solids with strong solids back-mixing that yields an exponential decay of the solids concentration with height); and located above these (iii) the transport zone (mainly composed of dispersed solids and exhibiting also exponential decay of the solids concentration, albeit at a lower back-mixing rate). This division of the solids flow into three fluid-dynamical regions has later on been confirmed in larger CFB boilers [7,14,15] and is today widely accepted. Yet, the conditions in the bottom bed, and thereby the splash zone, may differ between units, depending on furnace pressure drop, solids size distribution, operational condition and furnace geometry, such as if the lower part of the furnace has vertical or tapered walls. In addition, the bottom bed conditions in large boilers are difficult to determine since commercial boilers typically have only a few pressure taps for measurements of the pressure drop distribution along the furnace height. This can be seen from Fig. 1 which shows the vertical concentration profiles from different units in which the three regions can be identified, but which show differences between the units in the decay in solids concentration in the splash zone. The plotted profiles are derived from pressure measurements made at the furnace walls, which are typically regarded as providing a representative average solids concentration over the boiler cross-section [16–18]. The figure also illustrates the higher spatial resolution of the measurement data obtained from the Chalmers research unit (12-MW_{th}), as compared to typical datasets available from larger commercial units.

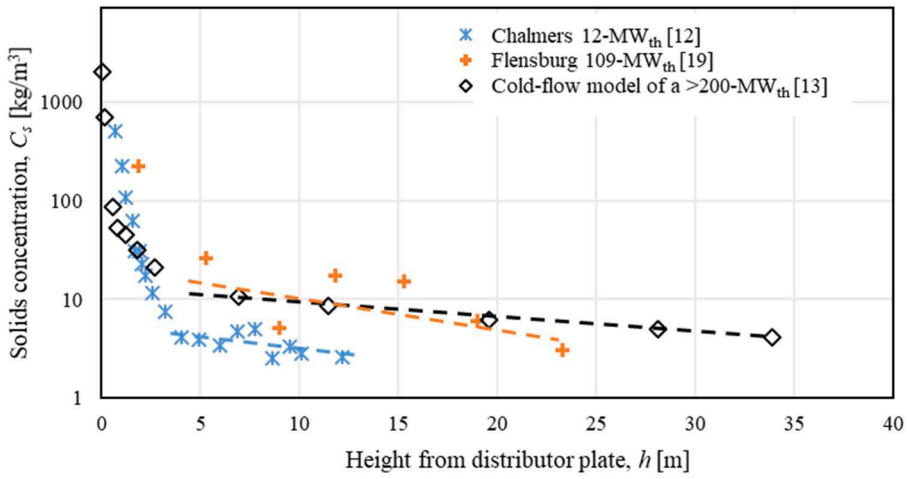

Fig. 1. Solids concentration profile derived from pressure measurements conducted at the walls in three CFB boilers. The values from the fluid dynamically downscaled cold model of a > 200-MW_{th} CFB boiler are upscaled. Single particle velocities are in the range of 2.4–3.0 m/s. Dashed lines cover measurements in the transport zone.

Shown also are the data from a cold-flow model operated according to scaling laws, which provides data of greater accuracy (i.e., a monotonic decay of solids concentration with height) than can be obtained in an industrial operation environment. The transport zone, which is the scope of the present study, extends from the end of the splash zone (at a height of 2–5 m) all the way up to the furnace exit (typically at a height > 30 m for commercial units). Thus, with the transport zone occupying most of the furnace (typically > 80% in large-scale units) and housing the major fraction of the heat-exchanging surfaces in the furnace, it becomes of crucial importance for the design and operation of large-scale CFB boilers to be able to describe the solids flow in this region. The overall characteristics of the transport zone is well established in units of different size where all units exhibits a core wall-layer solids flux with a relatively flat solids flux in the core and wall layers consisting of downward flowing solids which is assumed to constitute the main solids-backmixing in the transport zone[19–22].

Yet, despite the important role that solids back-mixing plays in the transport zone of large-scale CFB furnaces, it is poorly understood. The contributions of the different back-mixing paths, through the solids wall layers and *via* clustering, and how they are affected by unit size and shape, operational conditions and solids properties are largely unknown. As a consequence, there are no expressions in the literature that describe in macroscopic terms the solids back-mixing in the transport zone of CFB furnaces. This represents a major limitation for semi-empirical models and, thereby, for the adaptation of large-scale CFB technologies to new designs and applications.

The overarching aim of this work is to describe mathematically the solids back-mixing phenomena in the transport zone of large-scale CFB boilers. The specific objectives are to: (i) evaluate the contributions of the different solids back-mixing paths; (ii) define the governing transport phenomena underlying the dominant back-mixing path; and (iii) to derive a mathematical expression for the solids decay coefficient based on a more-solid theoretical ground than that used for previous expressions, so that it can be used in semi-empirical models.

This work applies to large-scale CFB combustors, which are typically characterized by: a furnace aspect ratio < 10; a dense bed (in the bottom of the furnace) aspect ratio that is much lower than 1; solids that belong to Geldart group B; and an external circulation of solids, G_s, that is < 20 kg/m^{2}s [14,21]. This work limits its scope to the solids flow in the transport zone, and thus does not include the bottom dense bed, splash zone or the exit zone.

2. Theory

The transport zone of large-scale CFB boilers exhibits decreases in the solids concentrations of roughly one order of magnitude (from around 10 kg/m^3 ($\varepsilon_s < 0.01$) to a value in the order of 1 kg/m^3 at the furnace top (i.e., $\varepsilon_s < 0.001$)). As mentioned above, the transport zone exhibits a relatively flat profile of the solids flux (kg/m^{2}s) across the horizontal direction, with the solids concentration decreasing moderately towards the wall layers. These features differ from those seen in narrow CFB units, e.g., FCC risers, which show much higher solids concentrations ($\varepsilon_s > 0.05$) [23], parabolic horizontal profiles of the solids flux [24,25] and, in some cases, the establishment of a solids flux with no net back-mixing, above a so-called 'transport disengagement height' [26]. To the best of the knowledge of the authors, such a terminal solids flow has not been observed in any of the solids concentration profiles derived from large-scale CFB boilers reported in the literature. Therefore, caution must be exerted when using the data from studies of narrow units for the analysis of large-scale CFB furnaces. Further, measurements in narrow CFB risers [27,28] show a clear particle size segregation effect along the height which is enhanced by wider size distribution of the solids inventory, while measurements in large-scale furnaces involve strongly poly-dispersed solids but are less conclusive in terms of solids size segregation along the transport zone [29]. Yet, the solids size segregation over the circulating loop is observed to decrease with an increase in gas velocity [12,29].

The solids flow in the transport zone of a large-scale CFB furnace follows a core/annulus flow structure [12,21,30], with a predominant upflow of dispersed solids in the core and a strong solids downflow at the furnace walls (the so-called 'wall layer'). The transfer of solids from the core region to the wall layer represents one back-mixing path for the solids. The fact that this transfer occurs from a low solids concentration (core) towards a denser one (wall layer) is studied in this work applying the hypothesis of a turbophoresis process. The boundary between the core region and the wall layers can be defined as the location at which the time-averaged solids flux in the vertical direction changes from an upward to a downward flux (the solids velocity can be used instead of the flux, yielding a slightly different point in space at which the average velocity changes direction [31]). As the core region feeds the downflow in the wall layer with solids, the thickness of the solids wall layer increases in the downward direction[21]. Measurements conducted in several commercial-scale CFB boilers [19,21,32] have shown a thicker wall layer in larger units. In summary, the core region occupies between 100% and 87% of the furnace cross-sectional area [14]. Given this fact and the uncertainty related to estimating the wall layer thickness, a widely applied simplification when studying the core region of large-scale CFB furnaces, used also in this work, is to assume that the cross-sectional dimensions of the core region are the same of those of the furnace.

As mentioned above, the upflow of dispersed solids in the core exhibits a relatively (though not perfectly) flat solids flux profile [19,21,24], although occasional downflow of solids has been observed also in this region [20,33]. Thus, the latter represents one potential pathway for back-mixing, and it can be explained by the clustering of the solids. However, it must be noted that once a cluster forms it will, providing it is large enough, descend due to the higher terminal velocity and after some distance it may break-up into dispersed particles which then start flowing upwards again by means of the drag from the upward flowing gas.

Fig. 2 schematizes the two possible paths for solids back-mixing cited above. The back-mixing through solids transfer to the wall layer (Path A) consists of two sequential transport mechanisms. Particles in the core region will eventually end up in proximity to the wall layer as a consequence of their lateral dispersive mixing, characterized by $D_{s,lat}$ (A.1) and driven by the large and vigorous fluctuating gas flow structures originating from the bottom bed dynamics, as discussed more in

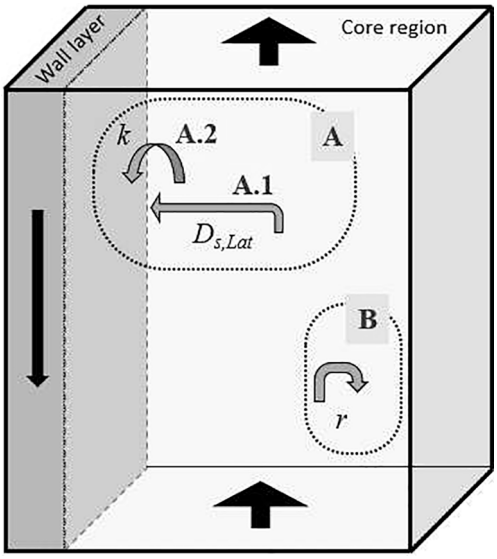

Fig. 2. Schematic of the solids back-mixing paths in the transport zone of a large-scale CFB furnace, showing implicated mechanisms (Path A, Path B) and governing parameters thereof.

detail in Section 2.1. Then, there is net transfer of these solids to the wall layers, which can be expressed by a net mass transfer rate k (A.2), after which the particles are back-mixed to the dense bed. Solids in the transport zone can also back-mix internally within the core region (Path B) by clustering at a net volumetric rate r, which results in clustered solids that fall downwards in the core region. The reason why clustering is required for back-mixing in the core region is that the superficial velocity in the transport zone typically exceeds the terminal velocity of all the solids (under typical full-load operating conditions).

Based on the scheme depicted in Fig. 2, the mass balance over the disperse solids in an arbitrary finite volume of the core region can be expressed. The difference in the upwards flow of disperse solids through the bottom and top of the volume is given by the total solids back-mixing, which consists of the sum of the particles transported from the core to the wall layer and the particles clustering in the core. Expressing this mass balance for the dispersed solids over a differential horizontal slice with height dh yields the following expression:

$$F_{in} - F_{out} = dF_{core \rightarrow layer} + dF_{clustering} \tag{1}$$

The disperse particles in the core region are assumed to flow according to their single-particle terminal velocity, i.e., the single-particle velocity is assumed to be u_g-u_t, an assumption that is supported by the measurements of Zhang et al. [20] (u_g is the superficial velocity based on the entire furnace cross-section, i.e., neglecting the wall layer thickness). The vertical dispersion of solids is neglected so as to simplify the analysis, which should be a reasonable assumption considering that the vertical single-particle velocity (typically > 2 m/s) is much higher than the effective dispersive velocity in the vertical direction ($\sim$0.1 m/s, as obtained from axial dispersion coefficients in the order of 1 m^2/s [34] and furnace heights > 10 m). The characteristic velocity for the lateral dispersion of solids within the core region can be expressed through the Einstein equation as follows:

$$u_{s,Dlat} = \frac{2D_{s,lat}}{\emptyset_h/2} \tag{2}$$

Eq. (1) can be developed into:

$$dC\left(u_g - u_t\right)A = C\left(\frac{\emptyset_h/2}{2D_{s,lat}} + \frac{1}{k}\right)^{-1}\frac{4A}{\emptyset_h}dh + CrAdh \tag{3}$$

where $4A/\emptyset_h$ corresponds to the perimeter of the horizontal slice (in Fig. 2). Note that the net core-to-wall layer mass transfer coefficient, k, is the net product of combining the transfer coefficient from the core to the wall layer and *vice versa*. Local solids flux measurements in CFB boilers [32] indicate that the core-to-wall layer transfer is much higher. Thus, the wall layer-to-core mass transfer is hereinafter neglected.

The analytical solution for the solids concentration in Eq. (3) is:

$$C(h) = c_1 e^{-Kh} \tag{4}$$

where the decay coefficient K is derived from:

$$K = \frac{\left(\left(\frac{\emptyset_h/2}{2D_{s,lat}} + \frac{1}{k}\right)^{-1}\frac{4}{\emptyset_h} + r\right)}{u_g - u_t} \tag{5}$$

This yields an exponential decay of the solids concentration with height, which is in agreement with observations made for all large-scale CFB furnaces reported in the literature and gathered in the present work (see Table 1). Equation (5) gives that the decay coefficient K depends on the furnace cross-sectional size and shape, the gas velocity, the solids properties, and the velocities/rates of the different mechanisms (k, $D_{s,Lat}$ and r), as illustrated in Fig. 2. The decay coefficient K has been the subject of several studies, ranging from its experimental evaluation to the formulation of empirical correlations. Regarding the latter, Johnsson and Leckner (have proposed the following expression based on measurements from the 12-MW$_{th}$ Chalmers boiler (covering the region u_g-$u_t \leq 3$) and three larger units (covering the region u_g-$u_t \geq 4.5$ and yielding lower values of K):

$$K = \frac{0.23}{u_g - u_t} \tag{6}$$

By accounting for experimental data from additional CFB boilers, Johansson et al. [7] have proposed an expression based exclusively on the geometry of the furnace:

$$K = \frac{1}{H_t} \tag{7}$$

Note that the furnace height in large-scale CFB boilers correlates closely with the furnace cross-section. This means that the empirical correlation given by Eq. (7) could indirectly express a dependency on the cross-sectional dimensions of the furnace.

The mechanisms in the freeboard that affect the concentration of solids in the furnace, as illustrated in Fig. 2, are further expanded upon in the following sections on lateral solids mixing and solids transfer to the wall layer.

It should be noted that solids backmixing also occurs at the furnace exit, where not all of the solids reaching the exit region are dragged by the gas out of the furnace and into the cyclone for external circulation, but a significant share (up to 80% in recent investigations in a cold flow model [13]) of the solids are internally back-mixed through the furnace wall layer.

2.1. Lateral solids mixing

The lateral mixing of solids is a major component of the flow pattern of the solids in the transport zone of large-scale CFB boilers [see Eq. (5)] and it also plays a central role in combustion and heat transport processes. Despite this, knowledge of this phenomenon remains very limited due to both the complexity of the experimental evaluation and the uncertainty related to CFD modeling results. The lateral mixing of solids is typically studied in terms of a dispersion coefficient, $D_{s,lat}$, corresponding to the A.1 mechanism depicted in Fig. 2 and describing the net dispersion of the particulate phase against the gas phase. The solids dispersion in the core region gas-solids flows is a consequence of both micro-scale transport (due to the fluctuations that result from the interactions between the gas and particles) and macro-scale motion [35,36]. Experimental work carried out in a 0.2 m-internal diameter (i.d.) CFB unit [37] revealed the solid dispersion coefficient to be of the same order of magnitude as that of the gas, although the solids mixing clearly varied with the solids concentration as a result of the particle interactions. Based on this limited evidence, the lateral solids dispersion coefficient in large-scale CFB boilers is often assumed to be equal to that estimated for the gas.

Bi et al. reviewed the CFB gas mixing literature and found that the lateral dispersion strongly increased with unit diameter, and they confirmed the above-mentioned lack of data for cross-sectional sizes larger than those employed for FCC reactors, i.e., reactors with diameters of a few decimeters [38]. Werther et al. [39] derived gas lateral dispersion coefficients from experiments carried out in a 0.4 m-i.d. riser operated with Geldart B solids under ambient conditions, and noted a strong dependency on the gas velocity. The experimental works of Sternéus et al. [24,35] have reported values for the lateral gas dispersion measured in units with direct relevance for commercial-scale CFB combustors. Importantly, the works of Sternéus et al. [24,36] have demonstrated that lateral gas mixing is strongly dependent upon unit size, i.e., higher values should be expected in utility-scale boilers than in the Chalmers 12-MW$_{th}$ CFB boiler ($\emptyset_h = 1.5$ m). Sternéus et al. have evaluated the lateral gas dispersion coefficient in the Chalmers 12-MW$_{th}$ CFB boiler ($\sim 10^{-2}$m^2/s) and in a cold-flow model operated with non-scaled solids ($\sim 5 \cdot 10^{-3}$m^2/s) [24]. Scaled solids were used in a later work using a cold-flow model of the Chalmers 12-MW$_{th}$ CFB boiler [35], which yielded values of around $5 \cdot 10^{-4}$m^2/s (these scale up nicely to the values of around 10^{-2} m^2/s found in the boiler). This revealed that the

presence of solids increased the lateral gas dispersion somewhat while still keeping it within the same order of magnitude as for single-phase flow. This was in line with previous findings [24,39] showing that the values for the lateral gas dispersion coefficient measured under CFB conditions were in reasonable agreement with those estimated using the *Pe*-number ranges for turbulent single-phase flow, i.e., $Pe = 250–1000$. Thus:

$$Pe = \frac{u_g \emptyset_h}{D_g} \tag{8}$$

Dispersion coefficients for both the gas and solids are a basic prerequisite for the modeling of large-scale CFB boilers using a semi-empirical approach (i.e., solving the balances for mass and heat but not that for momentum). Based on the experiments conducted by Kruse et al. [40] in a 0.4 m-i.d. riser, Lücke [41] used $Pe = 387$ in his modeling but noted that this underestimated the lateral gas dispersion when simulating the Chalmers 12-MW_{th} CFB boiler, instead discovering that to generate model results that were in good agreement with the measurements the *Pe*-number had to be decreased to 150. Wischnewski [42] also found that this decreased *Pe*-number yielded modeled data that were in better agreement with the measurements made in the furnace of the Duisburg 252-MW_{th} CFB boiler [42]. The possibility to satisfactorily describe dispersion in boilers of different sizes with one *Pe*-number suggests a linear, or close to linear, relation between the dispersion coefficient and the unit size. Macroscopic-scale motion, which is cited as the dominant mechanism for lateral dispersion in large-scale CFB boilers [43], has been proposed to be governed by large gas pockets that originate from bottom bed dynamics as the air bubbles/jets reach the dense bed "surface" and develop throughout the freeboard. These gas pockets/eddies were initially observed in small bubbling fluidized beds [44,45], and thereafter in narrow CFBs [46]. Subsequently, their presence was noted in commercial CFB boilers [43].

Based on this, Palchonok et al. [47] have presented expressions to estimate the macroscopic solids dispersion by means of turbulence theory, i.e. by relating the solids dispersion to the turbulent properties of the gas flow. According to this, the macroscopic solids dispersion in the lateral direction is proportional to the large-scale fluctuations of the gas flow, which in turn relate to the eddy size of the gas flow, l_e:

$$D_{s,lat} \propto \frac{u' \emptyset_h}{\sqrt{3}} \tag{9}$$

$$u' \propto (g U l_e)^{1/3} \tag{10}$$

Macroscopic gas flow structures (identified by a differing chemical composition and coupled to fluctuations in the pressure signal) were observed in the Chalmers boiler which has a much larger size than those in smaller units [43]. Further, measurements with an impact pressure probe in the Chalmers 12 MW CFB boiler and in the larger Turow 235 MW CFB boiler show stronger fluctuations in the larger unit at a given height [20,22], which the authors of this work assume to relate to the eddy size. Based on this, the eddy size is in this work assumed to correlate linearly with the size of the unit:

$$l_e \propto \emptyset_h \tag{11}$$

Combining Eqs. (9)–(11) gives:

$$D_{s,lat} \propto \frac{g^{1/3} U^{1/3} \emptyset_h^{4/3}}{\sqrt{3}} \tag{12}$$

Note that the dependency of the macroscopic lateral solids dispersion on the fluidization velocity expressed by Eq. (12) differs from the linear dependency expressed through the use of a constant *Pe*-number in Eq. (8), which was validated in narrow CFB risers [37]. This difference has been explained previously [47] as reflecting the fact that different mechanisms are at play on different length scales. Note that neither the use of *Pe*-numbers nor the turbulence-based expression in Eq. (12) include any influence of the solids size on the dispersion.

2.2. Solids transfer to the wall layers

The transfer of disperse solids from the core region areas in the vicinity of the wall layer to the wall layer itself (mechanism A.2 in Fig. 2) has not been studied in detail in the literature. There are, however, reports from studies that have estimated the net transfer coefficient, *k*, and proposed expressions for the net transfer coefficient. Similarly, the literature on lateral solids mixing is more abundant and mature for narrow CFB risers than it is for large-scale CFB furnaces. As core-to-wall layer solids transfer takes place against the solids concentration gradient, Brownian diffusion or stochastic dispersion is not a suitable description of this transport mechanism. Below, we briefly present two descriptions of the core-to-wall layer transfer in terms of turbophoresis and the *Sh*-number, and show that they are equivalent.

Turbophoresis is the phenomenon whereby particles migrate in the direction of decreasing turbulence level. This phenomenon has been found responsible for the deposition of solid particles towards the walls in turbulent channel flow [48–50] and is also observed for high-inertia particles representative of CFB solids [51,52]. From the turbophoretic theory, the deposition velocity (analogous to the core-to-wall layer solids transfer coefficient, *k*) is expressed as [48]:

$$k = -\frac{\rho_p d_p^2}{18\mu} \frac{\partial\left(\overline{v_y'^2}\right)}{\partial y} \tag{13}$$

where $v_y'^2$ is the fluctuation of the particle velocity in the direction of the turbophoretic flow [48]. Since the spatial gradient of the variance of the solids velocity is difficult to measure, it has been studied instead by means of CFD modeling [53]. Meantime, experimental investigations with multiphase flows (aerosol droplets) are relatively abundant and have matured into the following expressions for the turbophoretic deposition velocity, for particles in the transitory region between the diffusional and inertial regimes [Eq. (14)], on the one hand, and the inertial regime [Eq. (15)] on the other hand [54]:

$$k = 0.02 Sc_p^{-2/3} Re^{-1/8} u_g \text{ for } 0.3 < \tau_V^* < 20 \tag{14}$$

$$k = min\left[6 \times 10^{-5} \tau_V^{*2}, 0.01\right] u_g \text{ for } \tau_V^* > 20 \tag{15}$$

where the dimensionless relaxation time is expressed as: $\tau_V^* = \frac{\tau (u^*)^2}{\nu_g} = 0.01 \tau u_g^2 / \nu_g$ [54] with the shear velocity, u*, assumed to be 10% of the mean flow velocity. Included here are the relaxation time, τ, the gas velocity u_g and the kinematic viscosity of the gas ν_g.

These expressions derived from studies of turbophoresis with aerosols show strong similarities to the expressions derived from experimental work carried out in fluidized bed units to determine the core-to-layer mass transfer coefficient in narrow, fast fluidized risers. For the latter, assuming turbulent flow and using experimental data on the amplitude of the velocity fluctuations, Bolton and Davidson [55] found that:

$$k = \frac{0.1\sqrt{\pi} u'}{1 + \frac{St}{12}} \tag{16}$$

Based on this, Davidson [30] proposed a simplified expression that assumes $St \ll 12$ and $u' = 0.1 u_g$:

$$k = 0.01 \sqrt{\pi} u_g \tag{17}$$

Note the strong similarity between Eq. (17), which was derived experimentally in narrow CFB risers, and Eq. (15) for the upper limit of the deposition coefficient of inertial particles, which was derived from turbophoretic investigations.

An alternative way to generalize the information about mass transfer through boundaries is by means of Sherwood number (*Sh*) correlations.

The Linton-Sherwood correlation for mass transfer in dilute flows [56] (derived from the Dittus-Boelter *Nu*-correlation for internal turbulent flow in rectangular pipes) reads:

$$Sh_{LS} = \frac{k\emptyset_h}{D_{s,lat}} = 0.023Re^{0.83}Sc^{0.33} \quad (18)$$

Applying $Re = \frac{\emptyset_h(u_g-u_t)\rho_g}{\mu_g}$ and $Sc = \frac{\mu_g}{\rho_g D_{s,lat}}$ to Eq. (18) yields the following dependencies for the mass transfer coefficient:

$$k \propto Re^{0.83}Sc^{0.33}\frac{D_{s,lat}}{\emptyset_h} \propto \left(\frac{\rho_g}{\mu_g}\right)^{0.5}\left(u_g-u_t\right)^{0.83}D_{s,lat}^{0.67}\emptyset_h^{-0.17} \quad (19)$$

These dependencies for *k* obtained from *Sh*-correlations bear a strong similarity to those derived from turbophoretic investigations with liquid droplets in the transitional regime [Eq. (14)] when developed as:

$$k \propto Re^{-1/8}Sc^{-2/3} \propto \left(\frac{\rho_g}{\mu_g}\right)^{0.542}\left(u_g-u_t\right)^{0.875}D_{s,lat}{}^{0.667}\emptyset_h{}^{-0.125} \quad (20)$$

In summary, turbophoresis represents a valid explanation for the transfer of solids from the dilute core region to the denser wall layer. Expressions derived from experiments with aerosols (which, as mentioned above, have served as the main source for the study of turbophoresis) show strong similarities to the empirical expressions derived from CFB data and to the *Sh*-number expressions for mass transfer in internal turbulent flows.

Overall, the back-mixing consists of two pathways (depicted in Fig. 2), namely:

A) Back-mixing through the wall layers. This can be divided into two sequential mechanisms.

A.1 – Lateral dispersion of particles in the core region occurring according to a lateral dispersion coefficient, $D_{s,lat}$. To date, there have been no experimental reports on this parameter with relevance for large-scale CFB boilers. Modeling of such units in the literature has involved estimations of the lateral dispersion of solids through *Pe*-numbers, while an expression for the dispersion coefficient based on turbulence theory has been proposed.

A.2 – Core-to-wall layer transfer of solids occurring according to a net mass transfer rate, *k*. The solids mass transport between the core and wall layer is assumed to follow the same parameter dependencies as those seen in expressions for the deposition velocity of multiphase flows (e.g., aerosol droplets) and in *Sh*-expressions for internal single-phase flow, which are shown to be very similar.

B) Back-mixing through the core region. Particles in the upwards solids flow in the core region may cluster at a volumetric rate, *r*, and undergo back-mixing (falling downwards) in the core region itself. Although the clustering of solids in the core region of large-scale CFB furnaces has been confirmed experimentally, the extent of such clustering has not been quantified and, thus, its relevance in comparison to the back-mixing in the wall layers remains unclear.

3. Methods

This work combines the analysis of experimental data and the use of two different models: one 3-dimensional (3D) finite element for the closure of the mass balance of dispersed solids over the transport zone; and one 3D direct number simulation for the detailed fluid dynamics of the gas particles. Below, the procedure for evaluating the experimental data reported in the literature is presented, together with the governing expressions for the two types of models employed.

3.1. Experimental data

The experimental data are gathered from large-scale CFB boilers described in the literature in the form of vertical profiles of either the pressure or solids concentrations. Neglecting acceleration effects, pressure measurements can be recalculated into solids concentrations, $C_s = \rho_s(1-\varepsilon_g)$, through solving ε_g [17,57] from:

$$\Delta P = \left(\rho_s(1-\varepsilon_g)+\rho_g\varepsilon_g\right)g\Delta h \quad (21)$$

Evaluating the decay coefficient in the transport zone from the vertical profile of the solids concentration often entails the difficulty of selecting which data-points are included in the calculation. Commercial CFB boilers often have a limited number of pressure taps available (and, thereby, a limited number of solids concentration data-points) (for an example, see the red cross markers in Fig. 3). The evaluation of the decay coefficient in the transport zone (i.e., the spatial gradient of the data-points at greater heights in Fig. 3) increases its robustness as the number of data points is increased, while the inclusion of each data-point at a lower height increases the risk of distorting the evaluation as the effect of the splash zone starts to weigh in gradually. Thus, the value of the decay coefficient in the transport zone, *K*, is calculated as the average of the values for *K* obtained from different sets of experimental data-points considered to be in the transport zone. In this way, the values of *K* are based on evaluating the vertical profiles of the solids concentration or pressure reported in the literature, and the values presented here do not necessarily agree with what the authors of the original work would have obtained. Considering the uncertainty linked to the evaluation, the values of *K* (and the parameters derived therefrom) are, in this work, plotted with an error bar that extends from K_{min} to K_{max}. Obviously, the uncertainty related to the evaluation of *K* decreases with the spatial resolution of the pressure profiles and the accuracy of the pressure transducers are improved. Table 1 shows the values for the decay coefficient in the transport zone derived from data in the literature.

Note that the literature data used contain variations in several parameters that are not considered in the present analysis and that directly or indirectly influence the results, i.e., secondary air configuration and share, particle size distribution, presence of internal heat extracting devices, riser pressure drop, temperature, fuel type, etc.

3.2. Modeling of the mass balance over dispersed solids in the core region

To study the solids back-mixing path through the wall layers (Path A in Fig. 2) and, more specifically, compare the two constituent transport mechanisms (the lateral solids mixing, A.1, and the core-to-wall layer transfer, A.2), a steady-state 3D closure of the mass balance over the disperse solids in the core region of a parameterized CFB furnace is implemented. In the closure of such a mass balance, the different expressions for the lateral solids mixing presented in the theory Section 0 can be used and, depending on the resulting solids concentration fields, validated or discarded for the description of large-scale CFB furnaces.

The mass balance is closed using the finite element method and applying the convection–diffusion equation. The flow of disperse solids in the core consists of an upwards convective component ($u_z = u_g$-u_t) and lateral dispersion $D_x = D_y = D_{s,lat}$ (diffusion in the axial direction is neglected, $D_z = 0$). In the core region, the lateral mixing is assumed to follow a dispersive pattern owing to stochastic fluctuations that originate from turbulent structures. Assuming a steady state, the mass balance reads:

$$0 = \overline{\nabla}\cdot\left(D_{s,lat}\overline{\nabla}C_s\right) - \overline{\nabla}\cdot\bar{u}C_s \quad (22)$$

In the domain defined (representing the core region of the transport zone), the boundary conditions used are a given inlet concentration at the bottom of the domain, and a zero-concentration gradient at the top boundary. For the cells in the side boundaries (i.e., those representing the interface between the modeled core region and the wall layer), an outwards solids flux governed by the net mass transfer coefficient, *k* (i.e., expressed as the outwards velocity) is applied.

The resulting 3D solids concentration field can be averaged in the horizontal directions, yielding vertical profiles of the solids

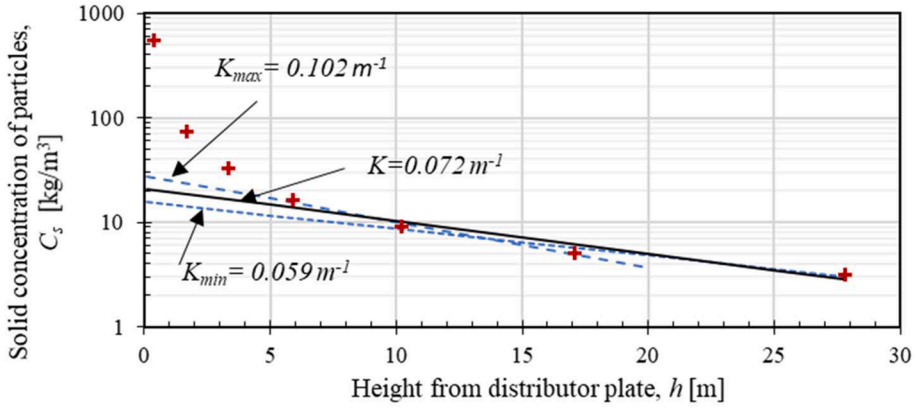

Fig. 3. Experimental solids concentration as obtained from pressure drop measurements in a 250-MW_e CFB unit [58] (red cross markers). The straight lines correspond to different fits to the solids concentration profiles, which yield the range of possible K-values shown in the plot.

Table 1
Decay coefficients in the transport zone derived from the literature [12,13,19,58-63], together with their plotting markers. The numbers indicated in red are approximated values.

Name	Capacity	L_x [m]	L_y [m]	$Ø_h$ [m]	H_t [m]	u_g [m/s]	dp [mm]	u_t [m/s]	$C_{s,min}$ [kg/m^3]	$C_{s,max}$ [kg/m^3]	K (K_{min}, K_{max}) [m^{-1}]
Chalmers [12]	12-MW_{th}	1.6	1.4	1.5	13.5	[2.7, 4.7]	0.2, 0.32	[1, 2.1]	2.6	40	0.325 (*0.173, 0.658*)
Flensburg [19]	109-MW_{th}	5.13	5.13	5.1	28	6.3	0.2	1.0	3	17	0.115 (*0.066, 0.161*)
Huchet [59]	125-MW_e	12.8	4.3	6.4	33	[4.8, 3.6]	0.25	1.5	1.6	36.6	0.079 (*0.044, 0.122*)
Örebro [60]	165-MW_{th}	12	4.7	6.8	33.5	4.6	0.27	1.7	1.7	5	0.057 (*0.015, 0.131*)
Duisburg [19]	105-MW_e	Diam	8	8	32	5.3	0.17	0.8	5.1	20.5	0.114 (*0.100, 0.122*)
Ref Boiler [13]	>200-MW_{th}	75 m^2		8.4	40	[3.5, 2.7, 2.2, 1.5]	0.19	1.1	0.5	12	0.069 (*0.034, 0.126*)
Cold-scale model [13]	>200-MW_{th}	75 m^2		8.4	40	[0.6-4.5]	0.195	1.1	0.1	25	0.057 (*0.043, 0.150*)
Zibo [61]	135-MW_e	13.1	6.6	8.8	38	[3.9, 4.0, 2.9]	0.17	0.8	2.5	64	0.111 (*0.066, 0.206*)
Gardanne [58]	250-MW_e	11.5	14.8	12.9	>36	5.2	0.3	1.9	3.2	16	0.078 (*0.059, 0.102*)
Turow [62]	235-MW_{th}	21.1	9.9	13.5	44	5.3	0.3	1.9	3.1	18.8	0.037 (*0.011, 0.053*)
Lagisza [63]	460-MW_e	10.6	27.6	15.3	48	[3.9, 3.0, 2.1, 1.6]	0.22	1.2	1.5	90	0.058 (*0.028, 0.206*)

concentration that exhibit an exponential fall-off with height in the furnace, from which the exponential decay coefficient K of the case simulated can be evaluated. This allows the study of how different combinations of the lateral solids dispersion, $D_{s,lat}$, and the core-to-layer mass transfer coefficient, k, generate different vertical decay constants for the solids back-mixing, K, and cross-sectional distributions of the solids concentration field.

3.3. Time-resolved modeling of the particle flow

To depict the detailed characteristics of the particle flow and test the hypothesis that turbophoresis is the mechanism governing the core-to-wall layer flow, we employ Direct Numerical Simulation (DNS) modeling. In this coupled Eulerian-Lagrangian approach, individual particles are tracked in a 3D turbulent channel. The carrier phase equations are the standard Navier-Stokes equations, including a forcing term that represents the particle feedback to the carrier phase. On the one hand, DNS has the advantage that it solves the flow equations without the approximation required in standard CFD simulations, where the turbulence models include approximations. On the other hand, this numerical framework comes with a substantial computational cost, and is limited to shorter dimensions of the computational domain and maximum simulation time following the evolution of the particle concentration in time, rather than along a spatial coordinate. Nonetheless, DNS allows us to perform detailed numerical simulations that solve down to the smallest flow scales driving the particle transport from the core to the wall layer, identifying all the physical quantities involved in this process.

The DNS results have been obtained with the pseudo-spectral Navier–Stokes solver SIMSON [64]. The streamwise and spanwise directions are discretized with Fourier series, while the wall-normal direction employs Chebyshev polynomials. Time integration is performed *via* a low-storage, three-stage, mixed Runge–Kutta/Crank–Nicolson scheme.

The flow transports particles that are evolved in a Lagrangian formulation inside the code. The forces acting on each particle are the non-linear drag [65] and gravity [66]. Particle feedback to the air is modeled *via* a particle-in-cell approach [67], while interparticle collisions are neglected, since we consider the upper diluted region of a fluidized bed. The temporal discretization of the particle dynamics is achieved using a second-order Adams–Bashforth method [68,69]. For the gas phase, the wall boundary is defined by no flux in the normal direction and no slip in the vertical direction, the opposite side applying a symmetric boundary (no flux in the normal direction), and the bottom and top having coupled flow boundaries, in order to respect the mass balance closure.

The model assumes that the particles are rigid spheres with a diameter of 0.33 mm and density of 2,600 kg/m^3, and that the gas is air at hot condition of 800 °C. A gas flow, corresponding to a superficial velocity of 5.8 m/s, is set as the initial condition for the gas phase.

Regarding the solids, a total of 1.536×10^8 particles is considered, yielding an average particle concentration of $2\,kg/m^3$, i.e., $\varepsilon_s = 0.0008$. The domain has cross-sectional dimensions of $1.442 \times 1.132\,m^2$ and a height of 2.265 m. Together with the connected bottom and top boundaries, this domain is assumed to represent the transport zone. The number of grid-points used in the simulations is around 150 million. The simulation data for a given time, t, is calculated as an average over 0.5 s, i.e., from $t - 0.25$ s to $t + 0.25$ s, and the total time simulated is 8 s.

4. Results and discussion

Fig. 4 shows the values of the decay coefficient K in the transport zone as obtained in the present work by evaluating the literature data from the large-scale CFB boilers listed in Table 1. Fig. 4 presents the K data as a function of the single-particle velocity, u_g-u_t and it is clear that most of the values lie within the interval of 0.02–0.2 m^{-1}. In line with what is reported in Section 3.1, there are significant uncertainties in determining K and no clear relationship to the single-particle velocity or the unit size is observed, with the exception of the Chalmers unit, which is by far the smallest unit and yields higher decay coefficients which is shown below to be due to the much higher perimeter-to-area ratio (in Eq. (23)).

In order to correlate the contributions of each of the two back-mixing paths (see Fig. 2) to the observed decay in solids concentration, the above-derived expression for the decay coefficient [Eq. (5)] can be reformulated to:

$$K(u_g - u_t) = \left(\frac{1}{k} + \frac{\emptyset_h/2}{2D_{s,lat}}\right)^{-1} \frac{4}{\emptyset_h} + r \tag{23}$$

Based on this, Fig. 5 plots the furnace data in Fig. 4 according to Eq. (23), with $4/\emptyset_h$ as the abscissa. The data in Fig. 5 clearly tend towards the point of origin (see the magnified region), indicating a weak contribution of the solids back-mixing in the core region due to cluster formation [the second right-hand term in Eq. (23), marked as B in Fig. 2], as compared to solids back-mixing in the furnace wall layers [the first right-hand term in Eq. (23), marked as A in Fig. 2].

As a consequence, the expression for the decay coefficient can now be simplified to:

$$K = \frac{\left(\frac{\emptyset_h/2}{2D_{s,lat}} + \frac{1}{k}\right)^{-1} \frac{4}{\emptyset_h}}{u_g - u_t} \tag{24}$$

4.1. Mass balance over dispersed solids in the core region

With the core-to-wall layer back-mixing path identified as the dominant pathway, we proceeded to investigate the interplay between the two constitutive transport mechanisms [the lateral solids dispersion within the core region; and the core-to-wall layer solids transfer (see Fig. 2)] by means of the closure of the mass balance presented in Section 3.2.

Initially, to study the validity of different expressions for the lateral solids dispersion given in the literature and presented in the Section 0, the mass balance is solved with very high (in the order of 10^{10} m/s) values for the mass transport coefficient, k. In this way, if the resulting decay coefficient is lower than the experimentally derived one, the lateral dispersion values used can be discarded, as they are shown to be too low to supply the wall layer with a sufficiently high flow of solids. In Fig. 6, for each plot, the region under the diagonal indicates that the lateral solids dispersion used is unable to mirror the experimental data, despite the infinite core-to-wall layer mass transport applied, i.e., the expression cannot provide valid descriptions of the large-scale CFB boiler data.

Fig. 6a evaluates the solids dispersion obtained for $Pe = 150$, i.e., the expression used to model the Chalmers boiler [41] and the Duisburg 252-MW_{th} CFB boiler [42]. As shown in Fig. 6a, the data-points corresponding to the Chalmers boiler fall within the validity region, although it is also evident that using $Pe = 150$ prevents the correct prediction of the vertical decay in solids concentration for the remainder of the boilers in the literature. Furthermore, Fig. 6b show the results from investigating the lowest lower Pe-number that leads to valid values for the lateral dispersion of solids in all the cases studied, The lowest value is $Pe = 26$. Note that this value is below the lower limit in the interval (250–1,000) that is typically used for single-phase flow and that was earlier proposed in the literature for narrow CFB risers.

In summary, the Pe-number needed in order to attain the level of solids backmixing measured in all of the large-scale CFB furnaces studied ($Pe = 26$) is much lower than value ranges reported in the CFB literature ($Pe = 150$–1000, see Section 2.1), i.e. showing the higher lateral dispersion $D_{s,lat}$ in CFB furnaces. This is in line with the fact that flat lateral profiles of the solids flux and concentration are a general observation in large CFB boilers [19,21,24,60]. This fact indicates that the lateral dispersion of solids (transport mechanism A.1 in Fig. 2) is faster than the transfer through the boundary between the core and wall layer regions (transport mechanism A.2 in Fig. 2). These two mechanisms can be quantitatively compared through an equivalent solids dispersion velocity (derived from the Einstein equation as $u_{disp} = \frac{2D_{s,lat}}{(L=)\emptyset_h/2}$) and the core-to-wall layer mass transfer coefficient, both having

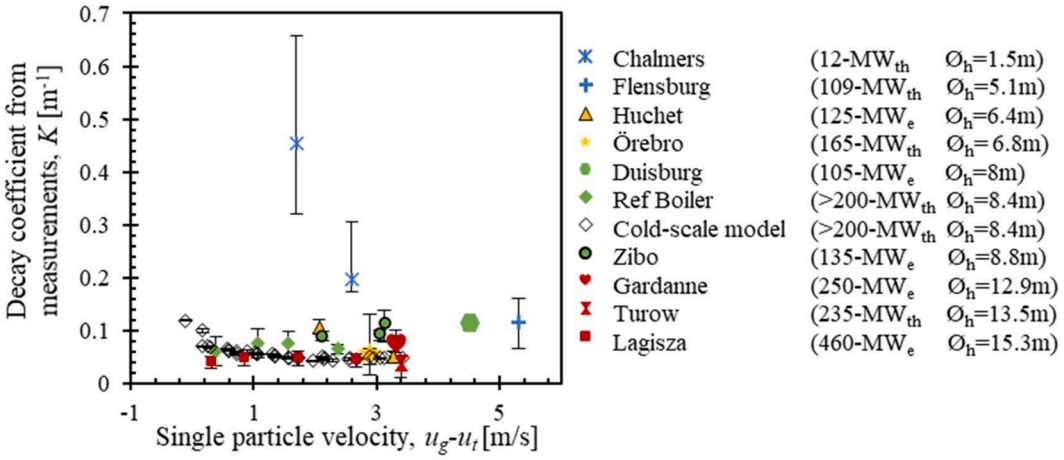

Fig. 4. Decay coefficients in the transport zones of large-scale CFB boilers. Calculated from the literature data (see Table 1).

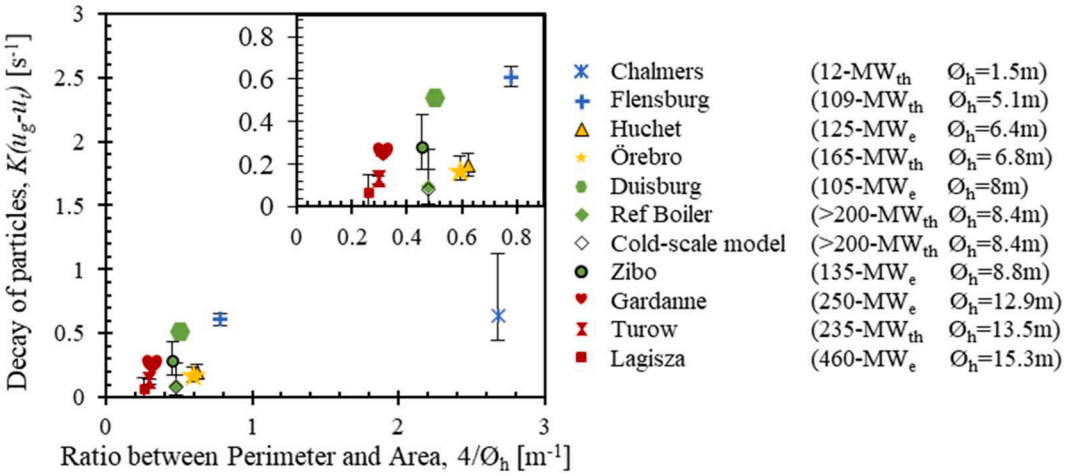

Fig. 5. The solids back-mixing rate (decay of particles, $K(u_g-u_t)$ as a function of the inverse unit size for different large-scale combustors.

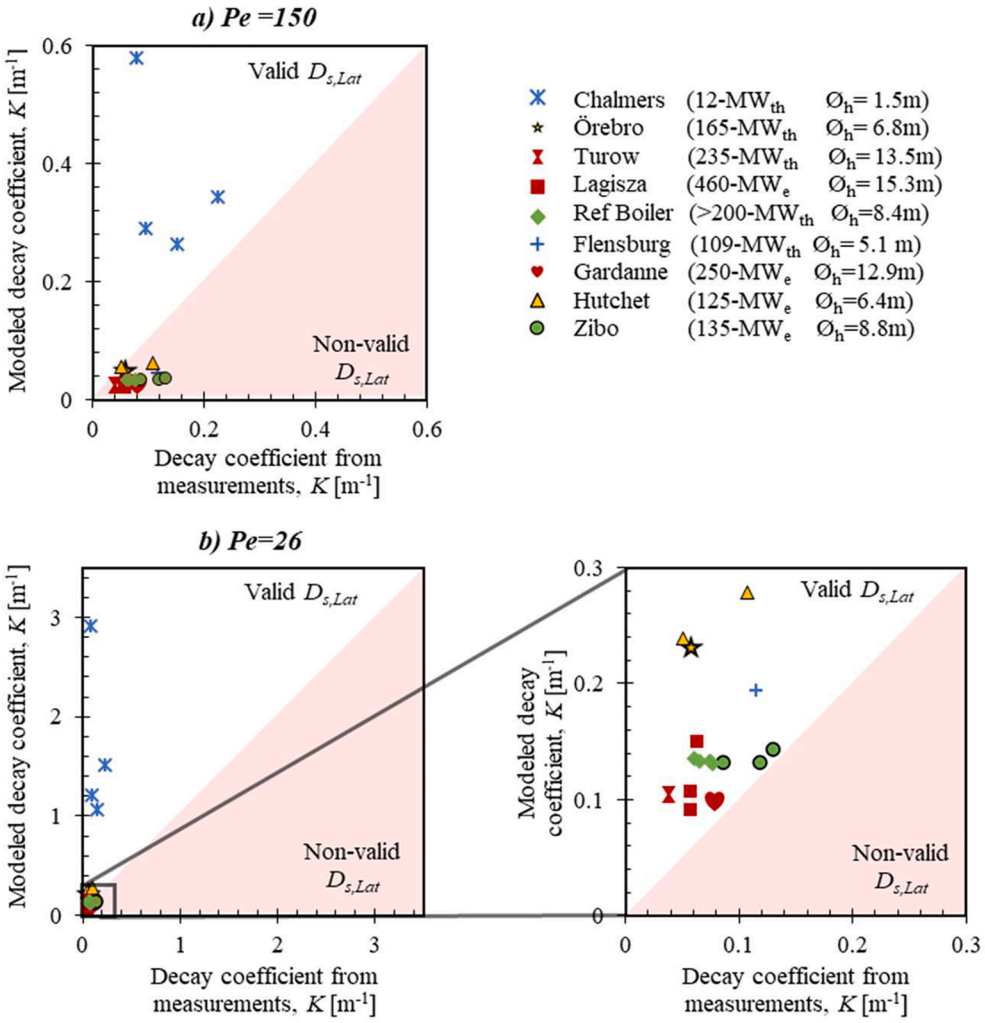

Fig. 6. Modelled decay coefficient values with quasi-infinite (10^{10} m/s) core-to-wall layer mass transfer, as compared to the decay coefficients based on measurements, for the indicated boilers. Solids lateral dispersion is estimated for: a) Pe = 150 [41]; b) Pe = 26 (lowest Pe-number able to provide the solids back-mixing required in all furnaces analyzed).

units [m/s]. A relatively flat horizontal solids profile in the core region corresponds to $u_{disp} \gg k$, which translates into:

$$D_{s,lat} \gg \frac{\emptyset_h}{4} k \tag{25}$$

Values for k can be derived from measurements in large-scale CFB furnaces showing flat lateral solids profiles in the core region according to the simplification of Eq. (24) into:

$$K = \frac{k \frac{4}{\emptyset_h}}{u_g - u_t} \tag{26}$$

Eq. (26) yields the data plotted in Fig. 7, where the core-to-wall layer mass transfer coefficient, k, approximately lies within the range 0.05–1 m/s. Setting these values in relation to Eq. (25) implies that the lateral solids dispersion in large-scale CFB furnaces needs to be driven by coefficients $D_{s,lat}$ significantly>0.05–2.7 m^2/s. This is in line with the above discussion in connection to Fig. 6. In summary, analysis of measurements in large-scale CFB boilers indicate that the lateral solids dispersion coefficient is much larger than the measured values for the lateral gas dispersion [24].

Further, Fig. 7 shows an approximately linear relationship between the mass transfer coefficient and the single-particle velocity (note the solids size is implicit in the latter through terminal velocity), together with a dependency on unit size (with smaller units tending to yield lower values). Note, however, the high level of uncertainty (large error bars) associated with many of the data-points, which is related to the low resolution of the pressure vertical profiles for most large-scale units described in the literature (see Section 3.1).

The calculated values for the core-to-wall layer transfer coefficients [Eq. (26)] derived from the decay coefficients in the large-scale CFB furnaces reported in the literature (*cf.* Table 1) are in the range of 0.01–1.0 m/s (Fig. 7). If restricting to those decay coefficients obtained under typical operating conditions, the mass transfer coefficients are in the range of 0.2–0.8 m/s, which are comparable to the values around 0.05 m/s reported in the literature for narrow CFB units [30]. Thus, expressions or values derived from smaller narrow CFB reactors typically render a serious underestimation of the core-to-wall layer solids transfer coefficients and cannot be used directly for quantitative descriptions of large-scale CFB furnaces [60].

4.2. Resolved modeling of the particle flow

Once the core-to-wall layer solids transfer was identified as governing the solids back-mixing in the transport zone of large-scale CFB furnaces, DNS modeling was employed to gain insights into the local characteristics of the particle flow and to evaluate the validity of turbophoresis as the mechanism underlying this solids transfer. The transient DNS simulation yields the formation and growth of a downflowing wall layer with much higher solids concentration than the upflowing core region.

Fig. 8a shows the establishment of a simulated flow picture that qualitatively resembles that derived from measurements in large-scale CFB boilers (for example, [21,60]). Thus, a wall layer with strong solids downflux and a core region with relatively low solids upflux and a rather flat horizontal profile are predicted (see Fig. 8a). From these profiles, the wall layer thickness can be evaluated as the location at which the time-averaged solids flux is zero (vertical lines in Fig. 8a). Note the increases in the wall layer thickness and solids downflux with time.

Fig. 8b shows the development with time of the simulated horizontal profiles for the variance of the solids velocity fluctuations in the horizontal direction. This is the parameter the spatial derivative of which governs the turbophoretic transport of solids [see Eq. (13)] [53]. It provides a more suitable explanation for the mass transfer of solids in the opposite direction than that given by the solids concentration gradient. The profiles in Fig. 8b are plotted with dashed lines, whereby the data obtained in the vicinity of the wall layer, but still in the core region (<30 mm), are plotted with thicker solid lines. From the latter solid segments, the local spatial derivative of the solids lateral velocity variance can be observed. It is clear that, despite the development of the wall layer in terms of thickness and solids flux with time, the cited spatial derivative at the core/layer boundary remains approximately constant (at a value of 0.166 [m/s^2]), which is in line with the constant mass transfer coefficient with height observed from measurements in large-scale CFB boilers. The DNS simulations indicate that the assumption that turbophoresis is the underlying mechanism for the core-to-wall layer mass transfer is reasonable. The phenomenon of thermophoresis, i.e. the migration of particles due to a temperature gradient, is assumed neglectable for the conditions relevant to this work. This, since the size of bed the material in the furnace yield a single particle mass about 10 orders of magnitude larger in comparison to particles shown to be affected by thermophoresis, e.g. soot and aerosols.

4.3. Prediction of the core-to-layer mass transfer coefficient

Based on the conclusion that the core-to-wall layer mass transfer governs the solids back-mixing in the transport zone of large-scale CFB furnaces and that this is based on a turbophoretic mechanism, the dependency expression given by Eq. (26) can be used to describe the mass transfer coefficient. Since the solids flow in commercial CFB furnaces is assumed to be dominated by the strong fluctuations that originate from the bottom region of the boiler, creating large eddies [18], a proportionality constant different to those used in Eqs. (14) and (15) is

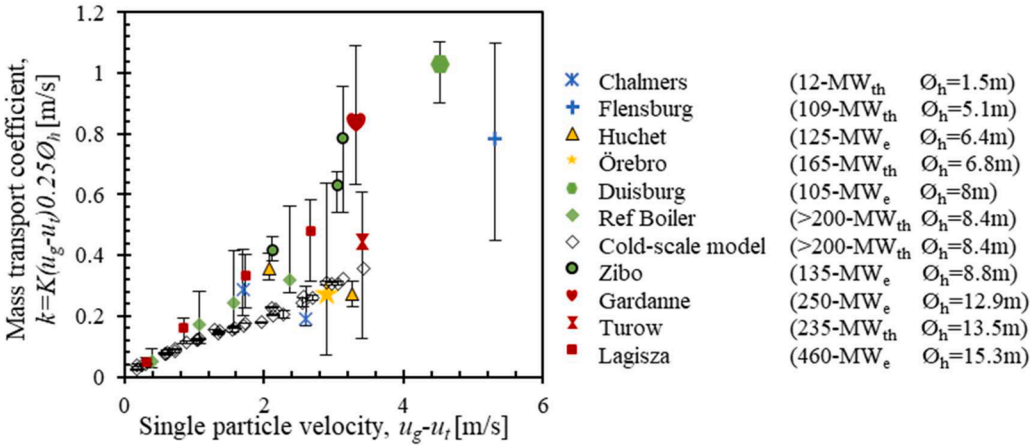

Fig. 7. Mass transport coefficients based on the measured K-values for each of the studied boilers.

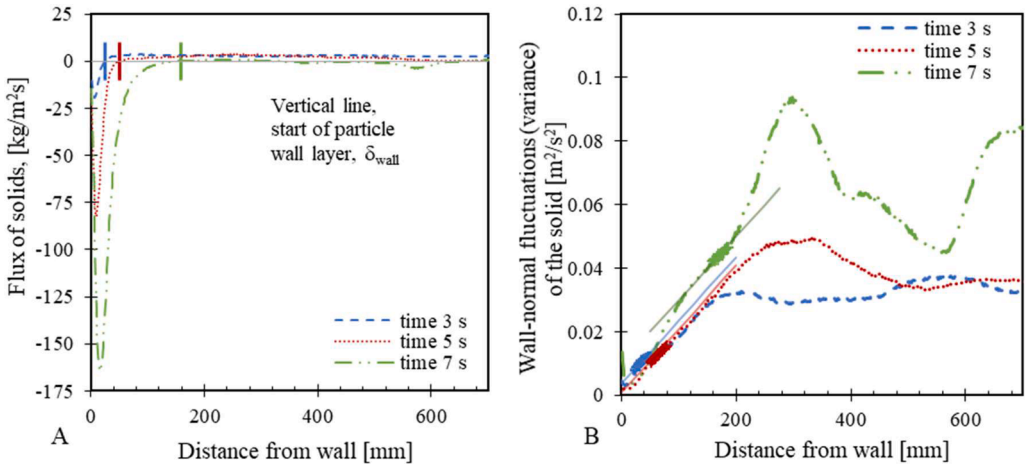

Fig. 8. a) Development of the simulated solids flux profile with time. b) Variance of the lateral solids velocity fluctuations at different simulation times.

expected.

Combining the dependency expression for the deposition velocity derived from the Linton-Sherwood correlation [Eq. (19)] with the expression for $D_{s,lat}$ provided by Palchonok and validated in Section 0 [Eq. (12)] results in:

$$k = C_1 \left(\frac{\rho_g}{\mu_g}\right)^{0.5} \left(u_g - u_t\right)^{1.05} \varnothing_h{}^{0.72} \tag{27}$$

Fitting the above expression to the mass transfer coefficients plotted in Fig. 7 (i.e., assuming perfect lateral mixing in the core region) yields a proportionality constant of $C_1 = 3.3{*}10^{-4}$. In addition, setting the gas properties to values typical for large-scale CFB combustion (here taken as $\rho_g = 0.33$ kg/m^3 and $\mu_g = 4.3{*}10^{-5}$ kg/m s) results in:

$$k = 0.029{*}\left(u_g - u_t\right)^{1.05}{*}\varnothing_h{}^{0.72} \tag{28}$$

The agreement for the correlation of the core-to-wall layer solids transfer coefficient proposed in Eq. (28) to the experimentally-derived values with Eq. (26) is shown in Fig. 9.

Combining Eqs. (26) and (28), the decay coefficient K can be written as:

$$K = 0.116{*}\varnothing_h{}^{-0.28}\left(u_g - u_t\right)^{0.05} \tag{29}$$

As shown, Eq. (29) yields an expression for the decay constant with a weak dependency on the single-particle velocity, which is in line with the data in Fig. 4. Furthermore, a slight inverse dependency on the unit size is obtained, in line with literature correlations that consider units of different size [7] [see Eq. (7)]. Fig. 10 shows the extents of agreement between the decay constants derived from experimental data and the different correlations proposed in the literature, including the one from this work [Eq. (29)]. The expression given in Eq. (29) yields an average difference with the measured values of 28%, which is to be compared with 280% for Eq. (6) [12], 86% for Eq. (17) used in Eq. (26) [30] and 57% for Eq. (7) [7].

5. Conclusion

The back-mixing of solids in the transport zone of large-scale CFB boilers is explored by combining modeling and experimental data from the literature, for 10 different large-scale CFB boilers.

The literature data exhibit variability regarding the solids concentration profile of the transport zone, including how the concentration falls off with height in the furnace (the decay coefficient K), which should be related to the low number of pressure taps in commercial CFB furnaces.

Processing of the experimental decay coefficients reveals that back-mixing *via* the wall layers is the dominant solids back-mixing pathway, surpassing the back-mixing within the core region caused by solids clustering.

Focusing on the back-mixing *via* the wall layers, the present study based on closures of a 3D mass balance modeling of the disperse solids in the core region shows that the core-to-wall layer mass transfer is the limiting (hence governing) transport mechanism, ahead of the much-faster lateral dispersion of solids within the core region. Thus, it

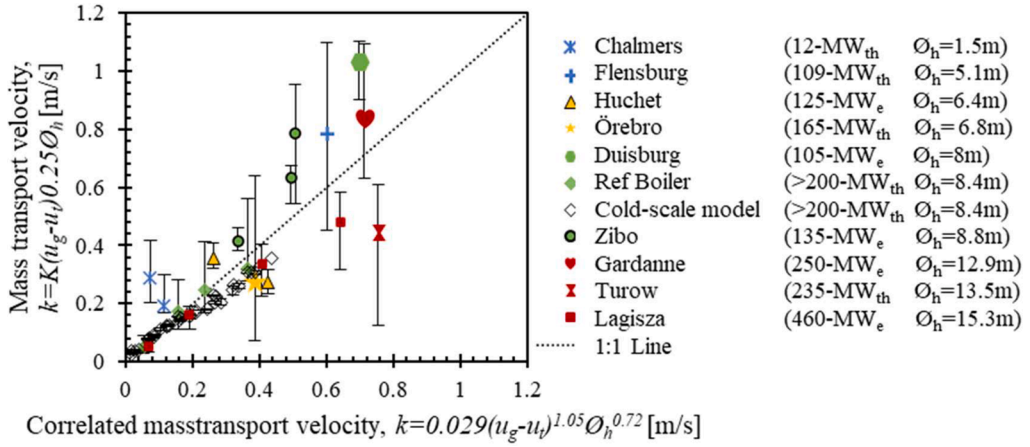

Fig. 9. Comparison of correlated [Eq. (28)] and experimentally derived [Eq. (26)] values of the core-to-wall layer mass transfer coefficient, k.

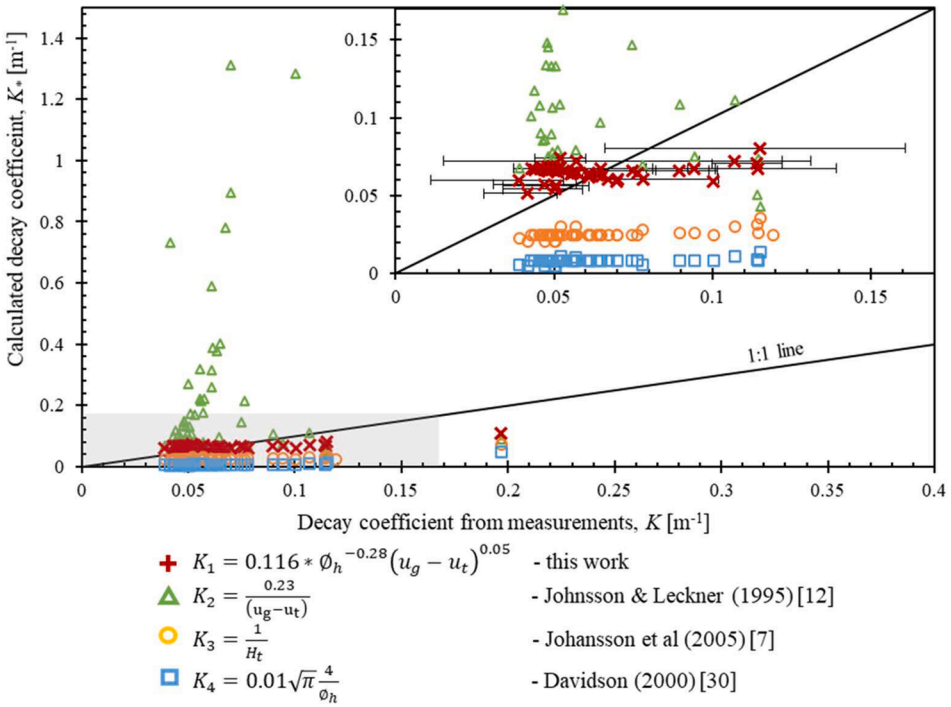

Fig. 10. Extent of agreement between the different expressions proposed in the literature, [including this work, Eq. (29)] and experimentally derived values. The gray area is magnified in the inset in the upper-right corner.

should be reasonable to assume that the core region is characterized by perfect lateral mixing of the solids. Furthermore, the mass balance closures show that *Pe*-numbers < 26 are needed to provide values of the lateral dispersion coefficient that are capable of describing the back-mixing measured in large-scale units.

The DNS simulations show that turbophoresis can be assumed to be the underlying mechanism describing the migration of solids from the core to the wall layer.

We propose an *Sh*-expression for the core-to-wall layer transfer of solids, and show that turbophoretic expressions yield similar dependencies. Based on this, an expression for the solids decay coefficient is proposed that yields better agreement with the experimental data from large-scale CFB furnaces than the correlations previously reported in the literature.

Declaration of Competing Interest

The authors declare that they have no known competing financial interests or personal relationships that could have appeared to influence the work reported in this paper.

Acknowledgments

We gratefully acknowledge the financial support from Valmet Technologies Oy within the framework for the project *Experimental investigation of the gas-solids flow in FB units* and from the Swedish Energy Agency within the framework for project 38347-2 (*Improved thermochemical conversion of biomass*).

References

[1] IEA, Energy, Climate Change and Environment 2016 Insights, I.E. Agency, Editor. 2016: Paris, France.
[2] Leckner, B., L. Thorson, J. Kjärstad, and F. Johnsson, Utilization of fluidized bed boilers —a worldwide overview, in Developments in Fluidized Bed Conversion 2011 to 2016. 2016, IEA-FBC TCP: Presented at IEA-FBC 73rd Technical Meeting, Tokyo, Japan (December 2016).
[3] Bo Leckner, Developments in fluidized bed conversion of solid fuels, Thermal science 20 (suppl. 1) (2016) 1–18.
[4] J Koornneef, M Junginger, A Faaij, Development of fluidized bed combustion—An overview of trends, performance and cost, Prog. Energy Combust. Sci. 33 (1) (2007) 19–55.
[5] Scala, F., Fluidized bed technologies for near-zero emission combustion and gasification. 2013: Elsevier.
[6] Sadegh Seddighi K., David Pallarès, Fredrik Normann, Filip Johnsson, Carbon monoxide formation during oxy-fuel-fired fluidized-bed combustion, Energy Fuels 27 (4) (2013) 2275–2282.
[7] Andreas Johansson, Filip Johnsson, Bo Leckner, Solids back-mixing in CFB boilers, Chem. Eng. Sci. 62 (1-2) (2007) 561–573.
[8] Robert C. Zijerveld, Filip Johnsson, Antonio Marzocchella, Jaap C. Schouten, Cor M. van den Bleek, Fluidization regimes and transitions from fixed bed to dilute transport flow, Powder Technol. 95 (3) (1998) 185–204.
[9] Bo Leckner, Fluidized bed combustion: mixing and pollutant limitation, Prog. Energy Combust. Sci. 24 (1) (1998) 31–61.
[10] Knowlton, T., Fluidized bed reactor design and scale-up, in Fluidized Bed Technologies for Near-Zero Emission Combustion and Gasification. 2013, Elsevier. p. 481-523.
[11] K. Myöhänen, T. Hyppänen, A three-dimensional model frame for modelling combustion and gasification in circulating fluidized bed furnaces, Int. J. Chem. Reactor Eng. 9 (1) (2011).
[12] Johnsson, F. and B. Leckner. Vertical distribution of solids in a CFB-furnace. in CONF-950522. 1995. American Society of Mechanical Engineers, New York, NY (United States).
[13] Tove Djerf, David Pallarès, Filip Johnsson, Solids flow patterns in large-scale Circulating Fluidised Bed boilers: experimental evaluation under fluid-dynamically down-scaled conditions, Chem. Eng. Sci. 231 (2021) 116309, https://doi.org/10.1016/j.ces.2020.116309.
[14] David Pallarès, Filip Johnsson, Macroscopic modelling of fluid dynamics in large-scale circulating fluidized beds, Prog. Energy Combust. Sci. 32 (5-6) (2006) 539–569.
[15] Jaap C. Schouten, Robert C. Zijerveld, Cor M.van den Bleek, Scale-up of bottom-bed dynamics and axial solids-distribution in circulating fluidized beds of Geldart-B particles, Chem. Eng. Sci. 54 (13-14) (1999) 2103–2112.
[16] J. Ruud van Ommen, Srdjan Sasic, John van der Schaaf, Stefan Gheorghiu, Filip Johnsson, Marc-Olivier Coppens, Time-series analysis of pressure fluctuations in gas–solid fluidized beds–A review, Int. J. Multiph. Flow 37 (5) (2011) 403–428.
[17] S Sasic, B Leckner, F Johnsson, Characterization of fluid dynamics of fluidized beds by analysis of pressure fluctuations, Prog. Energy Combust. Sci. 33 (5) (2007) 453–496.
[18] A. Svensson, F. Johnsson, B. Leckner, Bottom bed regimes in a circulating fluidized bed boiler, Int. J. Multiph. Flow 22 (6) (1996) 1187–1204.
[19] Werdermann, C.C., Feststoffbewegung und Wärmeübergang in zirkulierenden Wirbelschichten von Kohlekraftwerken. 1993: Shaker.

[20] Wennan Zhang, Filip Johnsson, Bo Leckner, Momentum probe and sampling probe for measurement of particle flow properties in CFB boilers, Chem. Eng. Sci. 52 (4) (1997) 497–509.
[21] Wennan Zhang, Filip Johnsson, Bo Leckner, Fluid-dynamic boundary layers in CFB boilers, Chem. Eng. Sci. 50 (2) (1995) 201–210.
[22] Johansson, A., F. Johnsson, B. Leckner, E.U. Hartge, J. Werther, R. Sekret, Z. Bis, W. Nowak, P. Noskievic, L. Strömberg, A. Kettunen, T. Hyppänen, and A. Hotta, Solids flow pattern in circulating fluidized-bed boilers. , in VGB PowerTech. 2004. p. 82–92.
[23] Chengxiu Wang, Jesse Zhu, John Grace, Xiaotao Bi, Naoko Ellis, Essentials of Fluidization Technology, Wiley, 2020, pp. 239–268, https://doi.org/10.1002/9783527699483.ch12.
[24] Johan Sternéus, Filip Johnsson, Bo Leckner, Gas mixing in circulating fluidised-bed risers, Chem. Eng. Sci. 55 (1) (2000) 129–148.
[25] Knöbig, T.C., Three-dimensional modeling of circulating fluidized bed combustion. 1998: Shaker.
[26] Hu, N., H. Yang, H. Zhang, R. Zhang, J. Cao, Q. Liu, J. Lu, and G. Yue. Experimental Study on Gas-Solid Flow Charcteristics in a CFB Riser Of 54M in Height. in Proceedings of the 20th International Conference on Fluidized Bed Combustion. 2009. Springer.
[27] Mitali Das, Meenakshi Banerjee, R.K. Saha, Segregation and mixing effects in the riser of a circulating fluidized bed, Powder Technol. 178 (3) (2007) 179–186.
[28] B. Hirschberg, J. Werther, Factors affecting solids segregation in circulating fluidized-bed riser, AIChE J. 44 (1) (1998) 25–34.
[29] Johnsson, F., C. Breitholz, and B. Leckner, Solids segregation in a CFB-boiler furnace, in Fluidization IX. 1998: Durango, Colorado, USA. p. 757-764.
[30] J.F Davidson, Circulating fluidised bed hydrodynamics, Powder Technol. 113 (3) (2000) 249–260.
[31] H.T. Bi, J. Zhou, S.Z. Qin, J.R. Grace, Annular wall layer thickness in circulating fluidized bed risers, The Canadian Journal of Chemical Engineering 74 (5) (1996) 811–814.
[32] Couturier, M., B. Doucette, D. Stevens, S. Poolpol, and V. Razbin. Temperature, gas concentration and solid mass flux profiles within a large circulating fluidized bed combustor. in 11th International Conference on FBC, ASME. 1991. Montreal.
[33] F. Johnsson, A. Johansson, J. Sterneus, An experimental study of in-furnace processes and dynamic behaviour of a 235 MWe CFB boiler, VGB powertech 84 (2004).
[34] Ronald W. Breault, A review of gas–solid dispersion and mass transfer coefficient correlations in circulating fluidized beds, Powder Technol. 163 (1-2) (2006) 9–17.
[35] J. Sternéus, F. Johnsson, B. Leckner, Characteristics of gas mixing in a circulating fluidised bed, Powder Technol. 126 (1) (2002) 28–41.
[36] J. Sternéus, F. Johnsson, B. Leckner, G.I. Palchonok, Gas and solids flow in circulating fluidized beds—discussion on turbulence, Chem. Eng. Sci. 54 (22) (1999) 5377–5382.
[37] R. Koenigsdorff, J. Werther, Gas-solids mixing and flow structure modeling of the upper dilute zone of a circulating fluidized bed, Powder Technol. 82 (3) (1995) 317–329.
[38] H.T. Bi, N. Ellis, I.A. Abba, J.R. Grace, A state-of-the-art review of gas–solid turbulent fluidization, Chem. Eng. Sci. 55 (21) (2000) 4789–4825.
[39] J. Werther, E.-U. Hartge, M. Kruse, Radial gas mixing in the upper dilute core of a circulating fluidized bed, Powder Technol. 70 (3) (1992) 293–301.
[40] M. Kruse, H. Schoenfelder, J. Werther, A two-dimensional model for gas mixing in the upper dilute zone of a circulating fluidized bed, The Canadian Journal of Chemical Engineering 73 (5) (1995) 620–634.
[41] K. Lücke, On the Influence if Mixing in the Performance of Large-Scale Atmospheric Circulating Fluidized Bed Combustors, Technischen Universit at Hamburg, Shaker, 2003.
[42] Wischnewski, R., Simulation of Large-Scale Circuating Fluidized Bed Combustors. 2008: Technischen Universität Hamburg.
[43] Fredrik Niklasson, Filip Johnsson, Bo Leckner, Local air ratio measured by zirconia cell in a circulating fluidised bed furnace, Chem. Eng. J. 96 (1-3) (2003) 145–155.
[44] Masayuki Horio, Hiroaki Kuroki, Three-dimensional flow visualization of dilutely dispersed solids in bubbling and circulating fluidized beds, Chem. Eng. Sci. 49 (15) (1994) 2413–2421.
[45] S.T. Pemberton, J.F. Davidson, Turbulence in the freeboard of a gas-fluidised bed: the significance of ghost bubbles, Chem. Eng. Sci. 39 (5) (1984) 829–840.
[46] Horio, M., A. Taki, Y. Hsieh, and I. Muchi, Elutriation and particle transport through the freeboard of a gas-solid fluidized bed, in Fluidization. 1980, Springer. p. 509-518.
[47] Palchonok, G., F. Johnsson, and B. Leckner, Estimates of turbulence effects in CFB boilers. Circulating Fluidized Bed Technology V, Science Press, Beijing, 1996: p. 440-445.
[48] Rajiv, K. and M.K. Lal, Turbophoresis, in Developments in Surface Contamination and Cleaning - Particle Deposition, Control and Removal. 2010: William Andrew Publishing.
[49] M. Caporaloni, F. Tampieri, F. Trombetti, O. Vittori, Transfer of particles in nonisotropic air turbulence, J. Atmos. Sci. 32 (3) (1975) 565–568.
[50] L.F. Mortimer, D.O. Njobuenwu, M. Fairweather, Near-wall dynamics of inertial particles in dilute turbulent channel flows, Phys. Fluids 31 (6) (2019) 063302, https://doi.org/10.1063/1.5093391.
[51] Y.A. Sergeev, R.S. Johnson, D.C. Swailes, Dilute suspension of high inertia particles in the turbulent flow near the wall, Phys. Fluids 14 (3) (2002) 1042–1055.
[52] Stefano Cerbelli, Andrea Giusti, Alfredo Soldati, ADE approach to predicting dispersion of heavy particles in wall-bounded turbulence, Int. J. Multiph. Flow 27 (11) (2001) 1861–1879.
[53] Cristian Marchioli, Maurizio Picciotto, Alfredo Soldati, Particle dispersion and wall-dependent turbulent flow scales: implications for local equilibrium models, J. Turbul. 7 (2006) N60, https://doi.org/10.1080/14685240600925171.
[54] Michaelides, E., C.T. Crowe, and J.D. Schwarzkopf, Multiphase flow handbook. 2016: CRC Press.
[55] L. Bolton, J. Davidson, Recirculation of particles in fast fluidized risers Circulating Fluidized Bed Technology, Elsevier, 1988, pp. 139–146.
[56] W. Linton, T. Sherwood, Mass transfer from solid shapes to water in streamline and turbulent flow, Chem. Eng. Prog. 46 (5) (1950) 258–264.
[57] F. Johnsson, S. Andersson, B. Leckner, Expansion of a freely bubbling fluidized bed, Powder Technol. 68 (2) (1991) 117–123.
[58] Leretaille, P., J. Werther, P. Briand, and D. Montat, Modeling of hydrodynamics of large scale atmospheric circulating fluidized bed coal combustors. 1999, Technical Univ. Hamburg-Harburg, Hamburg (DE).
[59] Lafanechere, L. and L. Jestin, Study of a circulating fluidized bed furnace behavior in order to scale it up to 600 MWe. 1995, American Society of Mechanical Engineers, New York, NY (United States).
[60] Johnsson, F., W. Zhang, and B. Leckner. Characteristics of the formation of particle wall-layers in CFB boilers. in Proceedings of the second international conference on multiphase flow. 1995. The Japan Society of Multiphase Flow Nagoya.
[61] Yang, H., G. Yue, X. Xiao, J. Lu, and Q. Liu, 1D modeling on the material balance in CFB boiler. Chemical Engineering Science, 2005. 60(20): p. 5603-5611.
[62] Johansson, A., Solids flow pattern in circulating fluidized-bed boilers. 2005.
[63] Mirek, P., Influence of the model scale on hydrodynamic scaling in CFB Boilers. Brazilian Journal of Chemical Engineering, 2016. 33(4): p. 885-896.
[64] Chevalier, M., A. Lundbladh, and D.S. Henningson, SIMSON–A pseudo-spectral solver for incompressible boundary layer flow, in Tech. Rep. TRITA-MEK 2007:07. 2007: KTH Mechanics.
[65] L. Schiller, A drag coefficient correlation, J Zeit. Ver. Deutsch. Ing. 77 (1933) 318–320.
[66] M.R. Maxey, J.J. Riley, Equation of motion for a small rigid sphere in a nonuniform flow, The Physics of Fluids 26 (4) (1983) 883–889.
[67] C.T. Crowe, M.P. Sharma, D.E. Stock, The particle-source-in cell (PSI-CELL) model for gas-droplet flows, ATJFE - ASME Transactions Journal Fluids Engineering 99 (1977) 325–332.
[68] G. Sardina, P. Schlatter, L. Brandt, F. Picano, C.M. Casciola, Wall accumulation and spatial localization in particle-laden wall flows, J. Fluid Mech. 699 (1) (2012) 50–78.
[69] Arash Nowbahar, Gaetano Sardina, Francesco Picano, Luca Brandt, Turbophoresis attenuation in a turbulent channel flow with polymer additives, J. Fluid Mech. 732 (2013) 706–719.